



Synthesis, structure and blue-light emission of a zero-dimensional zinc halide with the 4-(4-chlorophenyl)pyridinium cation

Ting Li and Hong-Ru Fu*

College of Chemistry and Chemical Engineering, Luoyang Normal University, Luoyang 471934, People's Republic of China. *Correspondence e-mail: hongrufu2015@163.com

Received 19 May 2025

Accepted 9 June 2025

Edited by X. Wang, Oak Ridge National Laboratory, USA

Keywords: pyridinium; tetrabromidozincate; crystal structure; zinc hybrid halide; pyridine cation; blue emission.

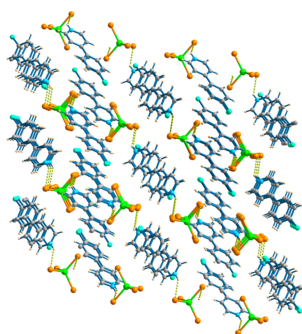
CCDC reference: 2452243

Supporting information: this article has supporting information at journals.iucr.org/c

Exploring blue emission lead-free halides with high photoluminescence quantum yields (PLQYs) is a significant and challenging issue for luminescent materials. Herein, a zero-dimensional (0D) organic-inorganic hybrid halide, namely, bis[4-(4-chlorophenyl)pyridinium] tetrabromidozincate, $(C_{11}H_9ClN)_2[ZnBr_4]$ or $[HCPP]_2[ZnBr_4]$ [CPP is 4-(4-chlorophenyl)pyridine], was synthesized through acid solution evaporation. The compound crystallizes in the monoclinic space group $C2/c$. The asymmetric unit consists of a $[ZnBr_4]^{2-}$ dianion cluster and two monoprotonated $[HCPP]^+$ cations. The $[ZnBr_4]^{2-}$ unit presents an almost undistorted tetrahedral geometry. The $[HCPP]^+$ cations adopt nearly coplanar conformations with small dihedral angles of $5.05(3)^\circ$; there are relatively strong $\pi-\pi$ interactions between adjacent $[HCPP]^+$ cations due to slipped parallel packing, with a distance of $3.81(1) \text{ \AA}$. Significantly, this halide exhibits highly efficient blue-light emission (385–500 nm) with a PLQY of 56.35%.

1. Introduction

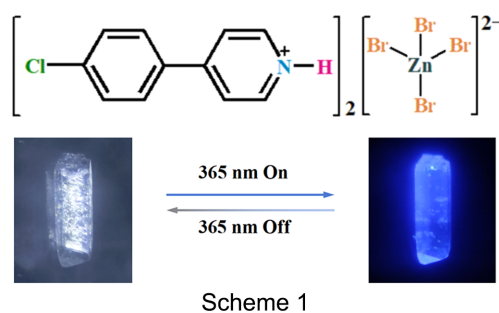
Recently, zero-dimensional (0D) metal hybrid halides have shown tremendous potential as luminescent materials due to their diverse structures and tunable photoluminescence (PL) (Han *et al.*, 2021; Haque *et al.*, 2025). Generally, 0D halides are composed of isolated metal halide clusters or units and bulky organic cations. In contrast to the high-dimensional halides, 0D hybrid halides always show strong quantum/dielectric confinement and possess much softer lattices, leading to an increased exciton binding energy, and allowing for the emission of self-trapped excitons (STEs) with wide broadband and large Stokes-shifted properties (Morad *et al.*, 2019; Dastidar *et al.*, 2024; Wang *et al.*, 2024a). As a result, lower-energy green, yellow and red light emissions are easily realized in 0D halides, while higher-energy blue-light emission remains extremely challenging, especially in the pure-blue region (460–480 nm) (Ma *et al.*, 2021; Zhang *et al.*, 2021; Yang *et al.*, 2025). Great effort has been made to explore the preparation of blue-emitting 0D halides. For instance, Lei and co-workers have reported a series of 0D hybrid zinc halides of the form $AZnBr_4$ [$A = 1$ -ethylpiperazine (EP), 1-phenylpiperazine (BP) and $N,N,2,2$ -tetramethylpropane-1,3-diamine (TMPDA)] based on discrete $[ZnBr_4]^{2-}$ tetrahedra exhibiting blue emission (452–485 nm) and a maximum photoluminescence quantum yield (PLQY) of 35.47% (Ma *et al.*, 2022a). Saparov and co-workers reported two halides, namely, (P-xd) $ZnCl_4$ and (P-xd) $CdCl_4$, where P-xd is *p*-xylylenediammonium, showing blue emission and a PLQY of 23% for (P-xd) $ZnCl_4$ (Popy *et al.*, 2023). This group also utilized trimethyl(4-stilbenyl)methylammonium



OPEN ACCESS

Published under a CC BY 4.0 licence

(R^+) as the organic cations to prepare indium(III) halides and the halide $R\text{InBr}_4$ displays high-efficiency blue emission with a PLQY value of 16.36% (Fattal *et al.*, 2021). In addition, Zhang's group prepared a 0D hybrid zinc halide, *i.e.* $(\text{C}_9\text{H}_{14}\text{N})_2\text{[ZnBr}_4\text{]}$ ($\text{C}_9\text{H}_{14}\text{N}^+$ is the *N*-butylpyridinium cation) based on the pyridine quaternary ammonium salt. This crystal shows efficient blue-light emission centred at 426 nm and a high quantum yield of 49.95% (Cheng *et al.*, 2023). Despite the significant achievements that have been made in the development of 0D lead-free halides, achieving highly efficient blue-light emission is extremely challenging due to the limitation of an intrinsic large Stokes shift and an unavoidable self-absorption effect (Ma *et al.*, 2022*b*; Peng *et al.*, 2021; Cho *et al.*, 2025). However, after summarizing the reported studies about blue-emitting 0D halides, we found that the construction of blue-emitting 0D halides is mainly concentrated on two strategies. The first common strategy is to adopt d^{10} metal ions, such as Zn^{2+} and Cd^{2+} , which have a relatively stable outer electronic structure (Liu *et al.*, 2024; Tan *et al.*, 2025; Hao *et al.*, 2022). The other is to focus on the modulation of organic cations. The organic components play a crucial role in generating blue emission and the introduction of an organic cation into a hybrid structure can improve its blue-emission efficiency (Deng *et al.*, 2023; Belikova *et al.*, 2024). These findings provide important inspiration for the design of hybrid halides as blue-light emitters.



In this study, a new 0D organic–inorganic hybrid halide, namely, bis[4-(4-chlorophenyl)pyridinium] tetrabromidozincate, $[\text{HCPP}]_2[\text{ZnBr}_4]$, was prepared by adopting chlorine-decorated 4-phenylpyridine as the cation source. This halide exhibits an intense blue emission centred at 432 nm through STEs of the $[\text{ZnBr}_4]^{2-}$ unit and a singlet excited state of the organic cations with a PLQY of 56.35%, surpassing almost all previously reported 0D zinc halide counterparts. This work provides an efficient way to achieve high-efficiency blue emission through the modulation of appropriate organics.

2. Experimental

2.1. Materials and methods

Zinc bromide (anhydrous, ZnBr_2 , 99.9%) and 4-(4-chlorophenyl)pyridine (CPP, 99.0%) were purchased from Alfa, and ethanol (EtOH, 99.9%) and hydrogen bromide (HBr, 35%) were purchased from Aladdin. All chemicals are used directly without further purification. Elemental analysis for C, N and H

Table 1

Experimental details.

Crystal data	
Chemical formula	$(\text{C}_{11}\text{H}_9\text{ClN})_2[\text{ZnBr}_4]$
M_r	766.27
Crystal system, space group	Monoclinic, $C2/c$
Temperature (K)	285
a, b, c (Å)	12.7583 (6), 14.1507 (5), 15.2706 (5)
β (°)	110.067 (1)
V (Å ³)	2589.57 (18)
Z	4
Radiation type	Mo $K\alpha$
μ (mm ⁻¹)	7.34
Crystal size (mm)	0.16 × 0.16 × 0.15
Data collection	
Diffractometer	Bruker APEXII CCD
Absorption correction	Multi-scan (<i>SADABS</i> ; Bruker, 2016)
$T_{\text{min}}, T_{\text{max}}$	0.321, 0.333
No. of measured, independent and observed [$I > 2\sigma(I)$] reflections	42246, 3223, 2597
R_{int}	0.074
$(\sin \theta/\lambda)_{\text{max}}$ (Å ⁻¹)	0.667
Refinement	
$R[F^2 > 2\sigma(F^2)], wR(F^2), S$	0.027, 0.067, 1.02
No. of reflections	3223
No. of parameters	145
H-atom treatment	H atoms treated by a mixture of independent and constrained refinement
$\Delta\rho_{\text{max}}, \Delta\rho_{\text{min}}$ (e Å ⁻³)	0.26, -0.61

Computer programs: *APEX2* (Bruker, 2016), *SAINT* (Bruker, 2016), *SHELXT* (Sheldrick, 2015*a*), *SHELXL2014* (Sheldrick, 2015*b*) and *OLEX2* (Dolomanov *et al.*, 2009).

was performed on an Elementar Vario MICRO instrument. Powder X-ray diffraction (PXRD) analysis was carried out with a Rigaku D/Max 2500 powder X-ray diffractometer using Cu $K\alpha$ radiation ($\lambda = 1.5418$ Å) at a voltage of 40 kV and 40 mA. Photoluminescence (PL) spectra, quantum yield and time-resolved decay spectra were recorded on an Edinburgh FLS1000 fluorescence spectrometer with a xenon lamp and an integrated sphere sample chamber.

2.2. Synthesis and crystallization

For the synthesis of $[\text{HCPP}]_2[\text{ZnBr}_4]$, a mixture of CPP (0.2 mmol) and ZnBr_2 (0.1 mmol) was dissolved in a mixture of ethanol (3 ml) and HBr (1 ml), and stirred at 353 K for 30 min. Colourless block-shaped crystals suitable for single-crystal X-ray diffraction analysis were obtained by slow evaporation under ambient conditions for 1 d. The crystals were collected, washed with acetone five times and then dried in air (yield 63.5%, based on Zn). Analysis calculated (%) for $\text{C}_{22}\text{H}_{18}\text{Br}_4\text{Cl}_2\text{N}_2\text{Zn}$: C 31.58, H 2.35, N 3.13; found: C 32.04, H 2.38, N 3.19.

2.3. Refinement

Crystal data, data collection and structure refinement details are summarized in Table 1. H atoms connected to C atoms were located at geometrically calculated positions.

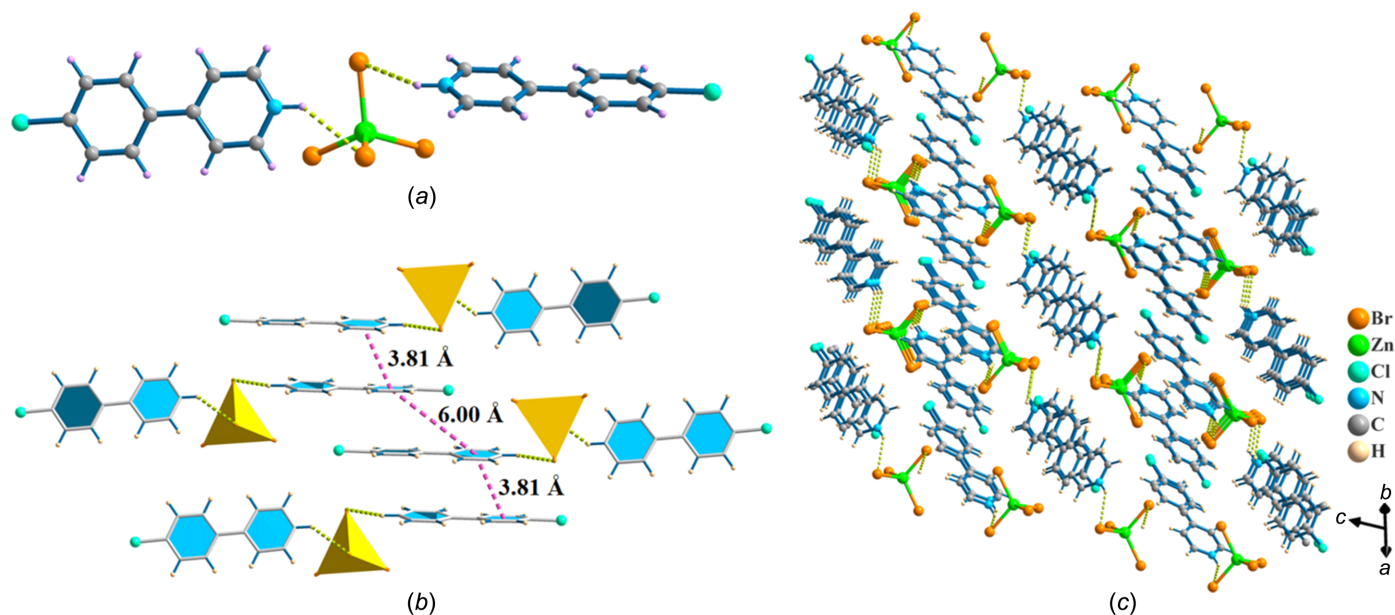


Figure 1
The molecular structure of $[\text{HCPP}]_2[\text{ZnBr}_4]$, showing (a) the tetrahedral $[\text{ZnBr}_4]^{2-}$ anion and $[\text{HCPP}]^+$ cation, (b) the interactions between the cations and inorganic nodes, and (c) a packing diagram of $[\text{HCPP}]_2[\text{ZnBr}_4]$.

2.4. Density Functional Theory (DFT) calculations

First-principles calculations were carried out using the projected augmented-wave (PAW) method (Kresse *et al.*, 1996), as implemented in *VASP* (Kresse *et al.*, 1999; Perdew *et al.*, 1992). The exchange correlation energy was treated using the Perdew–Burke–Ernzerhof (PBE) exchange–correlation functional in the scheme of generalized gradient approximation (Hohenberg *et al.*, 1964; Perdew *et al.*, 1996). The kinetic energy cutoff for all cases was determined to be 520 eV. The convergence thresholds for the electronic calculations and ionic relaxations were chosen as 10^{-6} eV and $0.01 \text{ eV } \text{Å}^{-1}$, respectively. The standard Monkhorst–Pack k-point grids with

a density of 0.1 Å^{-3} were used for Brillouin zone sampling. The valence electron configurations applied in this work were treated as Zn $3d^{10}4s^2$, C $2s^22p^2$, Cl $3s^23p^5$, Br $4s^24p^5$, N $2s^22p^3$ and H $1s^1$.

3. Results and discussion

Single-crystal X-ray diffraction analysis reveals that $[\text{HCPP}]_2[\text{ZnBr}_4]$ crystallized in the monoclinic space group $C2/c$. The asymmetric unit consists of two $[\text{HCPP}]^+$ cations and one $[\text{ZnBr}_4]^{2-}$ anion. As shown in Fig. 1(a), each Zn^{2+} ion is coordinated to four Br^- anions to form a $[\text{ZnBr}_4]^{2-}$ tetra-

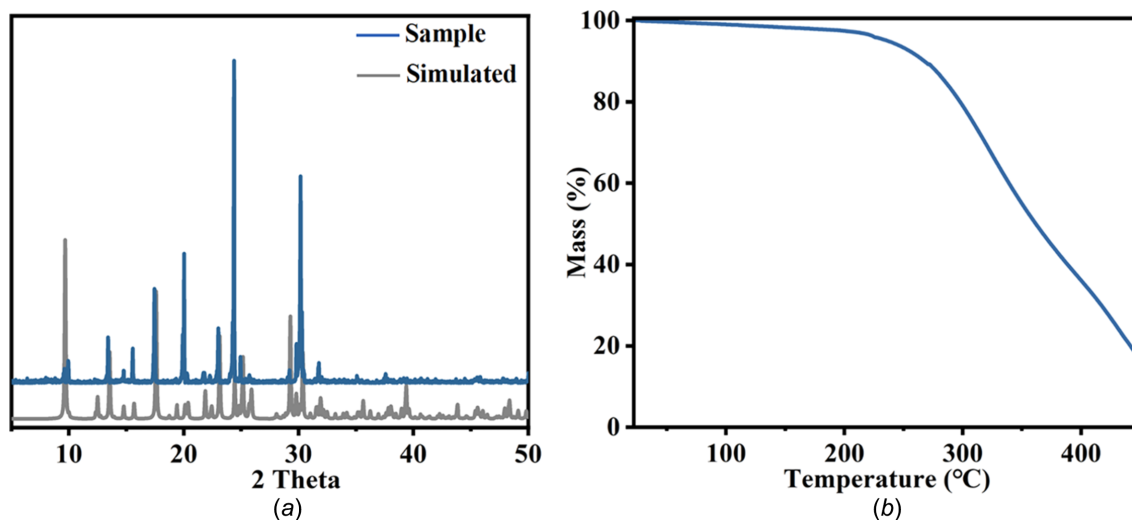


Figure 2
The basic characterization of $[\text{HCPP}]_2[\text{ZnBr}_4]$, showing (a) experimental and simulated PXRD patterns of $[\text{HCPP}]_2[\text{ZnBr}_4]$ and (b) thermal analysis of $[\text{HCPP}]_2[\text{ZnBr}_4]$.

hedron, yielding a zero-dimensional (0D) structure, with an average Zn–Br bond length of 2.4055 (4) Å and an average Cl–Zn–Cl bond angle of 109.04 (3)°, which are close to those of $[\text{ZnBr}_4]^{2-}$ tetrahedra in previously reported Zn-based hybrid halides (He *et al.*, 2023). Each $[\text{ZnBr}_4]^{2-}$ tetrahedron connects two $[\text{HCPP}]^+$ cations *via* intermolecular hydrogen bonds to form a 0D dimer; the Br \cdots H–N angle is 140.47 (3)°. One $[\text{HCPP}]^+$ cation of this dimer is arranged parallel to one $[\text{HCPP}]^+$ cation of another dimer, with an interplanar distance of 3.81 (1) Å [Fig. 1(b)]. These dimers are further stacked into a 3D supramolecular structure [Fig. 1(c)]. Notably, the pyridine and arene rings are nearly coplanar in the $[\text{HCPP}]^+$ cation, with a small dihedral angle between their planes of 5.05 (3)°. The degree of structural distortion of the ZnBr_4 tetrahedron was evaluated by calculating the distortion of the bond lengths (Δd) according to the equation of Robinson *et al.* (1971). The calculated Δd value is 1.14×10^{-4} and such a small degree of distortion (Liu *et al.*, 2023; Wang *et al.*, 2024b) suggests the weak STEs of the $[\text{ZnBr}_4]^{2-}$ cluster, which is good for the generation of the narrow emission band of $[\text{HCPP}]_2[\text{ZnBr}_4]$.

The powder X-ray diffraction (PXRD) pattern of $[\text{HCPP}]_2[\text{ZnBr}_4]$ matches well with that simulated from the obtained single-crystal data without any extra diffraction peaks, indicating their high purity [Fig. 2(a)]. The thermogravimetric (TG) curve shows that the $[\text{HCPP}]_2[\text{ZnBr}_4]$ crystals have

excellent thermal stability; they begin to decompose from ~ 250 °C [Fig. 2(b)].

The photophysical properties of $[\text{HCPP}]_2[\text{ZnBr}_4]$ were investigated. As shown in Fig. 3(a), the solid-state UV–Vis absorption spectrum of $[\text{HCPP}]_2[\text{ZnBr}_4]$ shows that the band edge is at about 400 nm. Upon 360 nm excitation, $[\text{HCPP}]_2[\text{ZnBr}_4]$ exhibits a narrow blue-emission band centred at 432 nm, with the full-width at half-maximum (FWHM) of 76 nm, a large Stokes shift of 46 nm and a high PLQY of 56.35%. The Commission Internationale de l'Éclairage (CIE 1931) chromaticity coordinates were determined as (0.16, 0.07) [Fig. 3(c)]. The PL decay lifetime is 1.76 ns at 432 nm [Fig. 3(d)].

In addition, the luminescence behaviour of CPP powder was tested and it exhibited a weak blue emission with a peak at 375 nm under 320 nm excitation [Fig. 3(b)], a PLQY of 11.36% and the CIE chromaticity coordinates (0.15, 0.06). The time-resolved spectrum of CPP under ambient conditions revealed a delay time of 0.86 ns at 375 nm [Fig. 3(d)]. Compared to the PLQY of CPP, the PLQY of $[\text{HCPP}]_2[\text{ZnBr}_4]$ shows a 4.96-fold improvement, which may be attributed largely to the ordered arrangement and rigid enhancement of CPP molecules in the halide matrix, leading to nonradiative transition suppression and PLQY improvements.

To better understand the luminescence mechanism of $[\text{HCPP}]_2[\text{ZnBr}_4]$, DFT calculations were performed to inves-

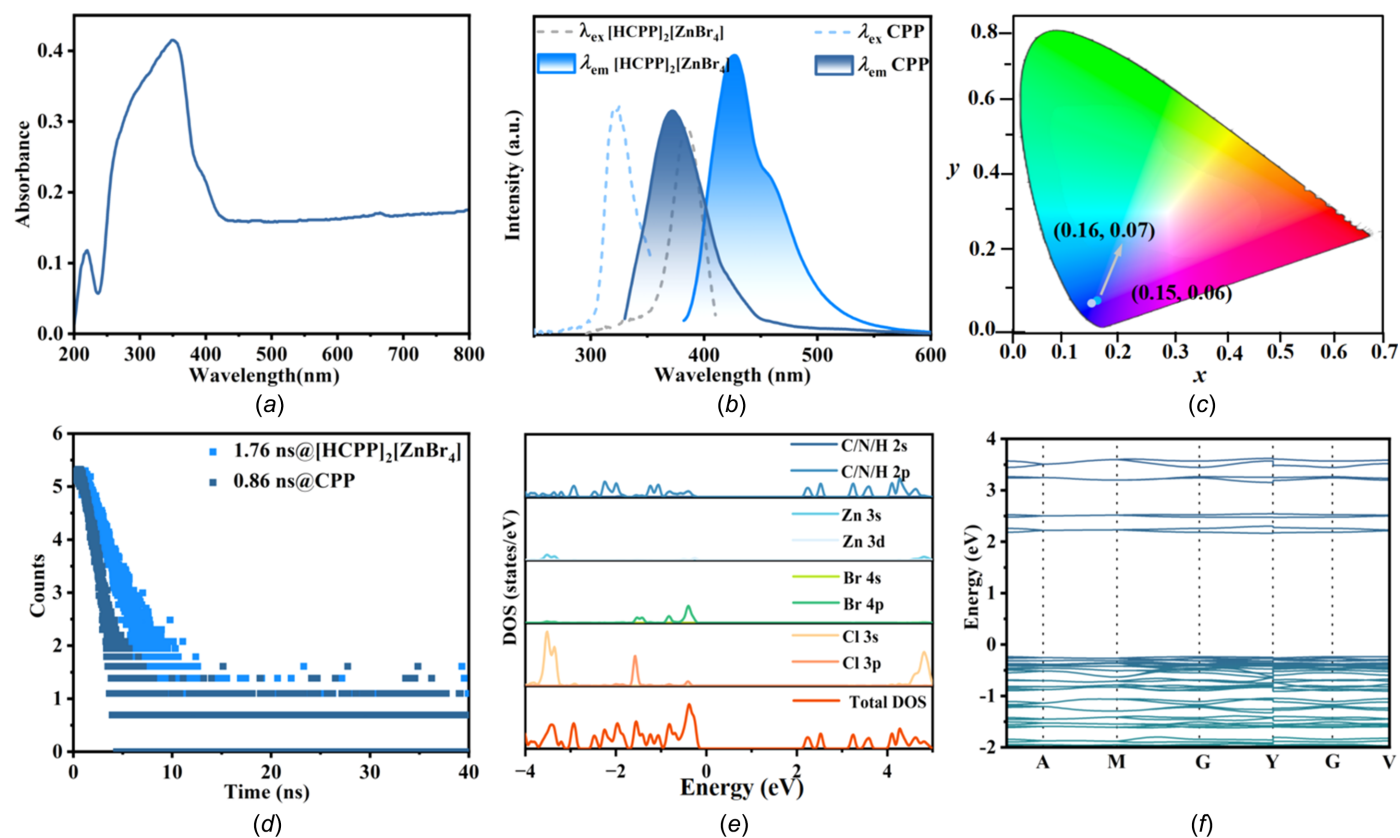


Figure 3

The luminescence properties and theoretical calculations for $[\text{HCPP}]_2[\text{ZnBr}_4]$, showing (a) the solid-state UV–Vis absorption spectrum of $[\text{HCPP}]_2[\text{ZnBr}_4]$, (b) the excitation and emission spectra of organic molecule CPP and $[\text{HCPP}]_2[\text{ZnBr}_4]$, (c) the CIE chromaticity coordinates, (d) the PL decay curves of CPP and $[\text{HCPP}]_2[\text{ZnBr}_4]$, (e) DOS and (f) calculated band structure.

tigate the band structure and density of states (DOS). The valence band maximum (VBM) of [HCPP]₂[ZnBr₄] is mainly located in the [HCPP]⁺ cation and the Br 4*p* orbital, and the conduction band maximum (CBM) is mainly distributed in the [HCPP]⁺ cation [Fig. 3(*e*)]. The energy band gap between the valence and conduction band of [HCPP]₂[ZnBr₄] is 2.48 eV [Fig. 3(*f*)], with such a small value indicating an intense quantum confinement effect. These results further confirm that the enhancement of blue emission of [HCPP]₂[ZnBr₄] originates from the organic cations and the STE of the [ZnBr₄]²⁻ node (Qi *et al.*, 2022).

4. Summary

By adopting chlorine-decorated 4-phenylpyridine, a zinc-based hybrid halide has been prepared. It exhibits efficient blue emission with a high PLQY of 56.35%, among the highest reported in the literature to date. Experimental and theoretical studies indicate that the emission originates from the synergistic function of the electron transitions in the organic cations and the STE states. This work lays the foundation for synthesizing more efficient blue-emission hybrid halides.

Conflict of interest

The authors declare that there are no conflicts of interests.

Funding information

Funding for this research was provided by: the Program for Innovative Research Team from the University of Henan Province (grant No. 24IRTSTHN005).

References

Belikova, D. E., Fateev, S. A., Khrustalev, V. N., Kozhevnikova, V., Ordinartsev, A. A., Dzuban, A. V., Goodilin, E. A. & Tarasov, A. B. (2024). *J. Mater. Chem. C* **12**, 13537–13544.

Bruker (2016). *APEX2, SAINT and SADABS*. Bruker AXS Inc., Madison, Wisconsin, USA.

Cheng, H., Hu, X., Cao, C., Li, X., Xie, R., Wang, D., Yang, W. & Zhang, Y. (2023). *J. Alloys Compd.* **968**, 171950.

Cho, S., Sree, V. G., Fulari, A. V., Park, S., Mei, M., Kim, M., Jana, A., Das, D., Im, H., Kyhm, K. & Taylor, R. A. (2025). *J. Colloid Interface Sci.* **680**, 215–225.

Dastidar, R. G., Okamoto, T., Takahashi, K., Takano, Y., Vijayakumar, C., Subrahmanyam, C. & Biju, V. (2024). *Nanoscale* **16**, 5107–5114.

Deng, Y., Liang, X., Li, F., Wang, M., Zhou, Z., Zhao, J., Wang, F., Liu, S. & Zhao, Q. (2023). *Laser Photonics Rev.* **17**, 2300043.

Dolomanov, O. V., Bourhis, L. J., Gildea, R. J., Howard, J. A. K. & Puschmann, H. (2009). *J. Appl. Cryst.* **42**, 339–341.

Fattal, H., Creason, T. D., Delzer, C. J., Yangui, A., Hayward, J. P., Ross, B. J., Du, M., Glatzhofer, D. T. & Saparov, B. (2021). *Inorg. Chem.* **60**, 1045–1054.

Han, Y., Yue, S. & Cui, B. B. (2021). *Adv. Sci.* **8**, 2004805.

Hao, X., Liu, H., Ding, W., Zhang, F., Li, X. & Wang, S. (2022). *J. Phys. Chem. Lett.* **13**, 4688–4694.

Haque, M. A., Grieder, A., Harvey, S. P., Brunecky, R., Ye, J. Y., Addison, B., Zhang, J., Dong, Y., Xie, Y., Hautzinger, M. P., Walpitage, H. H., Zhu, K., Blackburn, J. L., Vardeny, Z. V., Mitzi, D. B., Berry, J. J., Marder, S. R., Ping, Y., Beard, M. C. & Luther, J. M. (2025). *Nat. Chem.* **17**, 29–37.

He, S., Hao, S., Fan, L., Liu, K., Cai, C., Wolverton, C., Zhao, J. & Liu, Q. (2023). *Adv. Opt. Mater.* **11**, 2300218.

Hohenberg, P. & Kohn, W. (1964). *Phys. Rev.* **136**, B864–B871.

Kresse, G. & Furthmüller, J. (1996). *Phys. Rev. B* **54**, 11169–11186.

Kresse, G. & Joubert, D. (1999). *Phys. Rev. B* **59**, 1758–1775.

Liu, S., Wu, Y., Wu, J. & Lin, Z. (2024). *ChemPhotoChem* **8**, e202400139.

Liu, Y., Wang, W., Zhang, B., Wang, Y., Ren, M., Jing, Z. & Yue, C. (2023). *CrystEngComm* **25**, 444–449.

Ma, Y., Sun, Y., Xu, W., Liu, X., Zhong, Q., Song, Y., Fu, H., Yue, C. & Lei, X. (2022*a*). *Adv. Opt. Mater.* **10**, 2200386.

Ma, Y. Y., Fu, H. Q., Liu, X. L., Sun, Y. M., Zhong, Q. Q., Xu, W. J., Lei, X. W., Liu, G. D. & Yue, C. Y. (2022*b*). *Inorg. Chem.* **61**, 8977–8981.

Ma, Z., Shi, Z., Yang, D., Li, Y., Zhang, F., Wang, L., Chen, X., Wu, D., Tian, Y., Zhang, Y., Zhang, L., Li, X. & Shan, C. (2021). *Adv. Mater.* **33**, 2001367.

Morad, V., Shynkarenko, Y., Yakunin, S., Brumberg, A., Schaller, R. D. & Kovalenko, M. V. (2019). *J. Am. Chem. Soc.* **141**, 9764–9768.

Peng, H., Wang, X., Zhang, Z., Tian, Y., Xiao, Y., Hu, J., Wang, J. & Zou, B. (2021). *Chem. Commun.* **57**, 8162–8165.

Perdew, J. P., Burke, K. & Ernzerhof, M. (1996). *Phys. Rev. Lett.* **77**, 3865–3868.

Perdew, J. P., Chevary, J. A., Vosko, S. H., Jackson, K. A., Pederson, M. R., Singh, D. J. & Fiolhais, C. (1992). *Phys. Rev. B* **46**, 6671–6687.

Popy, D. A., Evans, B. N., Jiang, J., Creason, T. D., Banerjee, D., Loftus, L. M., Pachter, R., Glatzhofer, D. T. & Saparov, B. (2023). *Mater. Today Chem.* **30**, 101502.

Qi, Z., Gao, H., Zhu, X., Lu, Z. & Zhang, X. (2022). *Inorg. Chem.* **61**, 19483–19491.

Robinson, K., Gibbs, G. V. & Ribbe, P. H. (1971). *Science* **172**, 567–570.

Sheldrick, G. M. (2015*a*). *Acta Cryst.* **A71**, 3–8.

Sheldrick, G. M. (2015*b*). *Acta Cryst.* **C71**, 3–8.

Tan, R., Liu, Z., Zang, Z. & Zhao, S. (2025). *Chem. Sci.* **16**, 2136–2153.

Wang, Y., Kang, H., Zhang, S., Qu, H., Zhu, L., Zhao, D., Li, X., Lei, X. & Yue, C. (2024*a*). *Chem. Commun.* **60**, 2784–2787.

Wang, Y., Liu, J., Liu, Y., Li, S., Xu, X. & Lou, Z. (2024*b*). *J. Mater. Chem. C* **12**, 10267–10329.

Yang, C., Zheng, J., Xu, C., Xiao, C., Chang, Y., Zhou, L. & Gong, X. (2025). *Chem. Commun.* **61**, 4379–4382.

Zhang, F., Liang, W., Wang, L., Ma, Z., Ji, X., Wang, M., Wang, Y., Chen, X., Wu, D., Li, X., Zhang, Y., Shan, C. & Shi, Z. (2021). *Adv. Funct. Mater.* **31**, 2105771.

supporting information

Acta Cryst. (2025). C81, 462-466 [https://doi.org/10.1107/S2053229625005200]

Synthesis, structure and blue-light emission of a zero-dimensional zinc halide with the 4-(4-chlorophenyl)pyridinium cation

Ting Li and Hong-Ru Fu

Computing details

Bis[4-(4-chlorophenyl)pyridinium] tetrabromidozincate

Crystal data

(C₁₁H₉ClN)₂[ZnBr₄]

$M_r = 766.27$

Monoclinic, *C2/c*

$a = 12.7583$ (6) Å

$b = 14.1507$ (5) Å

$c = 15.2706$ (5) Å

$\beta = 110.067$ (1)°

$V = 2589.57$ (18) Å³

$Z = 4$

$F(000) = 1472$

$D_x = 1.965$ Mg m⁻³

Mo $K\alpha$ radiation, $\lambda = 0.71073$ Å

Cell parameters from 8684 reflections

$\theta = 2.3$ – 28.0 °

$\mu = 7.34$ mm⁻¹

$T = 285$ K

Block, clear light colourless

0.16 × 0.16 × 0.15 mm

Data collection

Bruker APEXII CCD
diffractometer

Radiation source: Bruker Nonius FR591
rotating anode

φ and ω scans

Absorption correction: multi-scan
(SADABS; Bruker, 2016)

$T_{\min} = 0.321$, $T_{\max} = 0.333$

42246 measured reflections

3223 independent reflections

2597 reflections with $I > 2\sigma(I)$

$R_{\text{int}} = 0.074$

$\theta_{\max} = 28.3$ °, $\theta_{\min} = 2.2$ °

$h = -17$ → 16

$k = -18$ → 18

$l = -20$ → 20

Refinement

Refinement on F^2

Least-squares matrix: full

$R[F^2 > 2\sigma(F^2)] = 0.027$

$wR(F^2) = 0.067$

$S = 1.02$

3223 reflections

145 parameters

0 restraints

Primary atom site location: dual

Hydrogen site location: mixed

H atoms treated by a mixture of independent
and constrained refinement

$w = 1/[\sigma^2(F_o^2) + (0.0318P)^2 + 1.6563P]$

where $P = (F_o^2 + 2F_c^2)/3$

$(\Delta/\sigma)_{\max} = 0.001$

$\Delta\rho_{\max} = 0.26$ e Å⁻³

$\Delta\rho_{\min} = -0.61$ e Å⁻³

Special details

Geometry. All esds (except the esd in the dihedral angle between two l.s. planes) are estimated using the full covariance matrix. The cell esds are taken into account individually in the estimation of esds in distances, angles and torsion angles; correlations between esds in cell parameters are only used when they are defined by crystal symmetry. An approximate (isotropic) treatment of cell esds is used for estimating esds involving l.s. planes.

Refinement. Data were collected using a using the Bruker D8 Venture with graphite-monochromated Mo $K\alpha$ radiation ($\lambda = 0.71073 \text{ \AA}$). The structures were solved by direct methods and refined by full-matrix least-squares on F^2 using the *SHELX2014* program (Sheldrick *et al.*, 2015) and *OLEX2* software (Dolomanov *et al.*, 2009). Non-H atoms were refined anisotropically.

Fractional atomic coordinates and isotropic or equivalent isotropic displacement parameters (\AA^2)

	<i>x</i>	<i>y</i>	<i>z</i>	$U_{\text{iso}}^*/U_{\text{eq}}$
Br1	−0.12018 (2)	0.60790 (2)	0.63802 (2)	0.04972 (9)
Zn1	0.0000	0.49763 (3)	0.7500	0.04242 (11)
Br2	−0.10686 (3)	0.40262 (2)	0.81686 (2)	0.06137 (10)
Cl1	0.64771 (8)	0.61203 (6)	0.37676 (7)	0.0784 (2)
N1	0.1419 (2)	0.66118 (16)	0.64135 (17)	0.0587 (6)
C3	0.30245 (19)	0.64480 (15)	0.55977 (16)	0.0433 (5)
C6	0.38753 (19)	0.63634 (16)	0.51485 (16)	0.0436 (5)
C9	0.5469 (2)	0.62288 (19)	0.4290 (2)	0.0548 (6)
C7	0.4910 (2)	0.68112 (19)	0.55141 (19)	0.0547 (6)
H7	0.5070	0.7161	0.6060	0.066*
C4	0.1950 (2)	0.60941 (19)	0.5179 (2)	0.0567 (6)
H4	0.1761	0.5792	0.4605	0.068*
C8	0.5702 (2)	0.6749 (2)	0.5088 (2)	0.0596 (7)
H8	0.6383	0.7057	0.5340	0.072*
C5	0.1172 (2)	0.6185 (2)	0.5600 (2)	0.0602 (7)
H5	0.0458	0.5943	0.5311	0.072*
C11	0.3673 (3)	0.5841 (2)	0.4329 (2)	0.0597 (7)
H11	0.2992	0.5537	0.4065	0.072*
C10	0.4467 (3)	0.5771 (2)	0.3909 (2)	0.0648 (7)
H10	0.4325	0.5416	0.3368	0.078*
C2	0.3221 (3)	0.6911 (2)	0.6442 (2)	0.0674 (8)
H2	0.3917	0.7181	0.6743	0.081*
C1	0.2415 (3)	0.6978 (2)	0.6838 (2)	0.0734 (9)
H1A	0.2568	0.7282	0.7408	0.088*
H1	0.087 (3)	0.663 (2)	0.669 (2)	0.081 (10)*

Atomic displacement parameters (\AA^2)

	U^{11}	U^{22}	U^{33}	U^{12}	U^{13}	U^{23}
Br1	0.04176 (14)	0.05317 (15)	0.05209 (15)	0.00680 (10)	0.01334 (11)	0.00912 (10)
Zn1	0.0411 (2)	0.0401 (2)	0.0461 (2)	0.000	0.01505 (16)	0.000
Br2	0.06093 (18)	0.05586 (17)	0.07050 (19)	−0.01307 (12)	0.02665 (14)	0.00854 (12)
Cl1	0.0741 (5)	0.0865 (6)	0.0936 (6)	0.0184 (4)	0.0533 (5)	0.0094 (4)
N1	0.0626 (15)	0.0559 (13)	0.0703 (15)	−0.0072 (11)	0.0391 (12)	0.0022 (11)
C3	0.0442 (13)	0.0350 (11)	0.0497 (12)	0.0008 (9)	0.0148 (10)	0.0039 (9)
C6	0.0440 (13)	0.0374 (11)	0.0487 (13)	0.0012 (9)	0.0152 (10)	0.0013 (10)
C9	0.0535 (16)	0.0524 (14)	0.0658 (16)	0.0134 (12)	0.0298 (13)	0.0103 (12)
C7	0.0499 (14)	0.0577 (15)	0.0560 (14)	−0.0033 (12)	0.0175 (12)	−0.0091 (12)
C4	0.0512 (15)	0.0592 (16)	0.0604 (16)	−0.0101 (12)	0.0201 (13)	−0.0115 (12)
C8	0.0405 (13)	0.0672 (17)	0.0726 (18)	−0.0011 (12)	0.0215 (13)	−0.0039 (14)

C5	0.0484 (15)	0.0617 (16)	0.0735 (18)	-0.0088 (12)	0.0248 (13)	-0.0001 (14)
C11	0.0575 (16)	0.0654 (17)	0.0588 (16)	-0.0125 (13)	0.0233 (13)	-0.0144 (13)
C10	0.0681 (19)	0.0719 (18)	0.0599 (16)	0.0000 (15)	0.0291 (14)	-0.0125 (14)
C2	0.0573 (17)	0.091 (2)	0.0570 (15)	-0.0194 (15)	0.0233 (13)	-0.0204 (15)
C1	0.079 (2)	0.090 (2)	0.0623 (17)	-0.0216 (18)	0.0384 (17)	-0.0209 (16)

Geometric parameters (Å, °)

Br1—Zn1	2.4312 (3)	C9—C10	1.372 (4)
Zn1—Br1 ⁱ	2.4312 (3)	C7—H7	0.9300
Zn1—Br2 ⁱ	2.3798 (3)	C7—C8	1.379 (4)
Zn1—Br2	2.3799 (3)	C4—H4	0.9300
Cl1—C9	1.737 (3)	C4—C5	1.361 (4)
N1—C5	1.318 (4)	C8—H8	0.9300
N1—C1	1.318 (4)	C5—H5	0.9300
N1—H1	0.93 (3)	C11—H11	0.9300
C3—C6	1.475 (3)	C11—C10	1.377 (4)
C3—C4	1.392 (3)	C10—H10	0.9300
C3—C2	1.390 (4)	C2—H2	0.9300
C6—C7	1.396 (3)	C2—C1	1.364 (4)
C6—C11	1.398 (4)	C1—H1A	0.9300
C9—C8	1.366 (4)		
Br1 ⁱ —Zn1—Br1	100.146 (18)	C3—C4—H4	119.6
Br2—Zn1—Br1	110.390 (10)	C5—C4—C3	120.8 (3)
Br2 ⁱ —Zn1—Br1 ⁱ	110.391 (10)	C5—C4—H4	119.6
Br2 ⁱ —Zn1—Br1	112.128 (10)	C9—C8—C7	119.0 (3)
Br2—Zn1—Br1 ⁱ	112.131 (10)	C9—C8—H8	120.5
Br2 ⁱ —Zn1—Br2	111.21 (2)	C7—C8—H8	120.5
C5—N1—H1	118 (2)	N1—C5—C4	120.7 (3)
C1—N1—C5	121.4 (3)	N1—C5—H5	119.6
C1—N1—H1	121 (2)	C4—C5—H5	119.6
C4—C3—C6	121.6 (2)	C6—C11—H11	119.5
C2—C3—C6	122.8 (2)	C10—C11—C6	121.1 (3)
C2—C3—C4	115.6 (2)	C10—C11—H11	119.5
C7—C6—C3	121.5 (2)	C9—C10—C11	119.7 (3)
C7—C6—C11	117.1 (2)	C9—C10—H10	120.2
C11—C6—C3	121.3 (2)	C11—C10—H10	120.2
C8—C9—Cl1	119.3 (2)	C3—C2—H2	119.3
C8—C9—C10	121.2 (3)	C1—C2—C3	121.3 (3)
C10—C9—Cl1	119.5 (2)	C1—C2—H2	119.3
C6—C7—H7	119.1	N1—C1—C2	120.1 (3)
C8—C7—C6	121.8 (2)	N1—C1—H1A	120.0
C8—C7—H7	119.1	C2—C1—H1A	120.0

Symmetry code: (i) $-x, y, -z+3/2$.